

**Interfacial reaction-induced roughening in polymer thin films**

Journal:	<i>Soft Matter</i>
Manuscript ID	SM-ART-01-2022-000150.R1
Article Type:	Paper
Date Submitted by the Author:	16-Mar-2022
Complete List of Authors:	Sengupta, Rajarshi; University of California Santa Barbara Tikekar, Mukul; University of California Santa Barbara, Materials Research Lab Delaney, Kris; University of California Santa Barbara Villet, Michael; Covestro Resins B.V. Fredrickson, Glenn; University of California Santa Barbara, Chemical Engineering & Materials

Interfacial reaction-induced roughening in polymer thin films

Rajarshi Sengupta¹, Mukul D. Tikekar², Kris T. Delaney¹,

Michael C. Villet³ and Glenn H. Fredrickson^{1*}

¹ Materials Research Laboratory, University of California Santa Barbara, Santa Barbara, CA, USA

² DSM Materials Science Center, Royal DSM, Geleen, The Netherlands

³ Covestro Resins B.V., Geleen, The Netherlands

Abstract

Reactive blending of immiscible polymers is an important process for synthesizing polymer blends with superior properties. We use a phase-field model to understand reaction dynamics and morphology evolution by diffusive transport in layered films of incompatible, end-reactive polymers. We thoroughly investigate this phenomenon over a large parameter space of interface shapes, layer thicknesses, reaction rates specified by a Damkohler number (Da_f), and Flory-Huggins interaction parameter (χ), under static conditions with no external fields. For films of the same thickness, the dynamics of the system is not significantly influenced by the length of the film or the initial shape of the interface. The interface between the polymers is observed to roughen, leading to the formation of a spontaneous emulsion. The reaction progresses slower and the interface roughens later for thicker films, and systems with higher χ . Increasing Da_f increases the reaction rate and hastens the onset of roughening. The quasi-static interfacial tension decreases with the extent of reaction, but does not become vanishingly small or negative at the onset of roughening. Simulations with reversible reactions and systems

*ghf@ucsb.edu

where only a fraction of the homopolymers have reactive end groups show that a critical diblock (reaction product) concentration exists, below which interfacial roughening and spontaneous emulsification is not observed. We also demonstrate that thermal fluctuations accelerate the onset of interfacial roughening, and help sustain the system in an emulsified state.

1 Introduction

Blending of immiscible polymers is an important process, which often produces polymer alloys having superior properties to the original polymers. This can be achieved by externally adding a copolymer to the system to compatibilize the immiscible polymers. Another strategy is to synthesize polymer with reactive endgroups, which react during processing to produce copolymer at the interface between the homopolymers [1, 2]. This technique of producing copolymers *in-situ* is called reactive polymer blending, and is widely employed industrially [1, 3]. The copolymer reduces the interfacial tension between the polymers, allows smaller domain sizes to be achieved, and improves adhesion between the homopolymer phases. Reactions are limited to the interfacial manifold separating the two initially incompatible resins being compounded. The reaction rate accelerates as the shear forces reduce the domain sizes, thereby expanding the interfacial area. The creation of copolymer at the interface further reduces the interfacial tension and reinforces the effect of shear and extensional forces in driving down domain size. Ultimately, the transport limitations are sufficiently reduced and enough copolymer is created to enable the system to spontaneously emulsify [4–10]. Complete conversion to block or graft copolymer is possible in systems with stoichiometric balance and irreversible reactions. A wide range of blend microstructures are observed, ranging from ordered mesophases formed by block copolymer-rich compositions, e.g. lamellae or hexagonally packed cylinders, to emulsion structures and co-continuous morphologies [11–15].

Theoretical models have been developed to predict the reaction kinetics of homogeneous and inhomogeneous end-coupling reactions [16–19]. The forward reaction between the homopolymers is modeled as a second order reaction in the homopolymer concentrations, and the backward reaction, if any, is modeled as first order in the copolymer concentration. In the absence of convection, the homopolymers near the interface react, and the reaction rate is initially controlled by the re-

action rate coefficient. This regime ends when the reactants in the vicinity of the interface are depleted, and further reaction is then controlled by the rate of diffusion of reactants from the bulk homopolymer phases to the interface. At even later stages, the copolymer brush at the interface presents a potential barrier to the reactants. The reaction rate progressively decreases through three regimes. Specifically, the interfacial coverage of the copolymer increases linearly with time in the first regime, followed by a growth proportional to the square root of time in the second regime, and an even slower growth as the square root of the logarithm of time in the final regime [18]. The reaction kinetics increases under flow for irreversible reactions having a dilute concentration of reactants [19].

Numerous experimental studies have been performed to measure the reaction rate constants [20], determine the reactivity of different chemical end groups [1, 21], compare the effectiveness of copolymer architecture [1], and quantify the effect of polymer-polymer interactions as measured by the Flory-Huggins interaction parameter, χ [1, 7, 22, 23]. It has been established that the copolymer generation rate and morphology evolution is controlled by the rate of interfacial area generation [9, 24]. Comparing the reaction rates for systems with and without flow, it was concluded that the interfacial area generated from shear forces alone was not sufficient to explain the large reaction rates observed in experiments [24]. It was hypothesized that another mechanism exists, in addition to external shear, which generates interfacial area for the progress of the reaction.

Experiments have been performed on static systems, with no external fields to determine the mechanism of interfacial area generation [4–10]. These studies usually employed either a film of one homopolymer cast on top of the second homopolymer, or slightly mixed homopolymers. The progress of reaction was monitored by observing the interface between the homopolymers using atomic force microscopy (AFM), or transmission electron microscopy (TEM). It was found that for many systems, the interface between the homopolymers became corrugated, eventually roughening and forming a spontaneous emulsion, generating enormous interfacial area. The spontaneous emulsification occurred when the interfacial excess diblock, as measured by forward recoil spectrometry (FRES) exceeded a critical value. Self consistent mean field calculations predicted the interfacial tension at the critical interfacial excess to become zero. The instability has been primarily attributed to the vanishing interfacial tension [4–6, 8], although some studies suggest that the reduction in interfacial tension is overestimated and argue that interfacial deformation caused by

thermal fluctuations also plays an important role in roughening and emulsification [7, 9, 25]. This phenomenon was observed for systems characterized by intermediate values of χN_r , where N_r is the relevant chain length. It was also observed that thinner films of homopolymers are more prone to roughening and spontaneous emulsification than thicker films [7, 26–28].

A fundamental understanding of spontaneous emulsification is necessary to control the system microstructure [28]. Although there have been numerous experimental works reporting interfacial roughening and emulsification, simulations predicting this phenomenon are scarce. The interface between segregated polymers was studied using molecular dynamics (MD) simulations, and observed to roughen [29]. The time scales accessed by MD simulations was no more than 1 ms due to the high computational resources demanded by the method. This was overcome using coarse-grained models like the dissipative particle dynamics (DPD) model [30–32], and a hybrid model which adopts a continuum description of the binary mixture and a particle description of the reactive molecules [33]. These approaches simulated time scales long enough to observe the onset and growth of interfacial roughening. The simulations determined the growth of the copolymer layer at the interface, and verified the different regimes predicted by theory [18]. However, there are disagreements on the cause of the instability. The hybrid model measured the total gradient energy to provide a rough estimate of the interfacial tension. In both the MD and DPD studies, the interfacial tension was calculated by measuring the difference between the normal and tangential components of the pressure tensor across the interface. Studies based on MD simulations and the hybrid model found the interfacial tension to drop to near zero or even negative values before the interface roughened, and attributed the vanishing interfacial tension as the cause of roughening [29, 33]. The DPD simulations, on the other hand, concluded that roughening is a microphase separation that occurs when the interface gets saturated with copolymer, and the system transitions to a lamellar microstructure [30, 31]. The interfacial tension was not observed to drop significantly in the DPD simulations at the onset of roughening. A likely reason for the disagreement is that there is no unambiguous way to calculate the interfacial tension in heterogeneous mixtures, particularly in non-equilibrium processes where interfaces are continuously changing.

The reactive blending process involves a complex interplay of thermodynamic forces, and multi-component and multi-phase transport; consequently, the parameter space that governs this process is daunting. Most simulations predicting spontaneous emulsification were focused on flat

interfaces of a constant thickness. A computational study that thoroughly investigates the evolution of copolymer, system morphology and interfacial roughening over a wide set of parameters is lacking. Recently, we developed a phase-field model to describe the reaction-diffusion processes occurring in the reactive blending process [34]. Phase field models combine the thermodynamics and transport of the system of interest, and are capable of describing non-equilibrium processes in inhomogeneous systems without the need to resolve highly constrained molecular degrees of freedom that limit accessible time scales in particle-based models, or track interfaces like the conventional techniques in fluid dynamics [35]. Such models have been employed previously for a wide range of problems in polymer physics [36, 37] and fluid mechanics [38, 39] like shear-induced demixing [40–42] in polymer solutions and nonsolvent induced phase separation [35, 43–45].

In this work, we employ the phase-field model developed previously to thoroughly investigate spontaneous emulsification for films of polymers containing reactive end groups, over a wider parameter space than has been previously reported. We determine the effects of interface shapes, film thicknesses, reactivity of end groups, reversible reactions, concentration of reactants, weak thermal fluctuations, and the Flory-Huggins parameter on the progress of the reaction and onset of interfacial roughening. We also investigate mechanisms for the origin of interfacial roughening. This work is limited to homopolymers symmetric in length and composition, which undergo an end-coupling reaction to form a diblock copolymer having length twice that of the homopolymers. Further, we focus only on reaction-diffusion, and defer the effects of convection to a future work. In section 2, we briefly describe our model and the phase-field method. We present the results and discussion in section 3. Finally, we present our conclusions in section 4.

2 Model

The reactive blending process is described using a multi-fluid model that has been derived and characterized in previous publications [34, 35, 43–45], and will be briefly reviewed in this section. The multi-fluid model is based on the two-fluid formalism of Doi and Onuki [46] and accurately describes the thermodynamics and kinetics of the system. We consider a mixture of two homopolymers, A and B, whose volume fractions are denoted by ϕ_{Ah} and ϕ_{Bh} , respectively, and that can reversibly or irreversibly react at a single end to form an A-B diblock copolymer. The diblock

copolymer concentration is denoted by ϕ_D . The homopolymers are assumed to have the same chain length, thus the diblock is twice as long as the homopolymers, and the mixture is assumed to be incompressible. The two blocks of the diblock are tracked with their own concentration fields (ϕ_{Ad} and ϕ_{Bd}), in order to specify their relative locations in space and capture microphase separation. The total diblock concentration is, $\phi_D = \phi_{Ad} + \phi_{Bd}$.

The chain lengths of the polymers are scaled with a reference chain length, N_r , which is equal to the length of the homopolymers. The radius of gyration obtained from the reference polymer length, $R_g = b\sqrt{N_r/6}$ is chosen as the characteristic length scale, where b is the monomer length. The Rouse time, $\tau_R = R_g^2/D$ is chosen as the reference time scale, where the self diffusion coefficient is $D = k_B T/N_r \zeta_0$. Here k_B is the Boltzmann constant, T is the temperature, and ζ_0 is the friction coefficient of the monomer. Thus, the characteristic time scale is $\tau_R = N_r^2 b^2 \zeta_0 / 6 k_B T$. The Damkohler number is calculated from the rate constant k_f of the forward reaction, $Da_f = k_f \tau_R = k_f N_r^2 b^2 \zeta_0 / 6 k_B T$, and is the ratio of diffusion to reaction time scales [47]. The equilibrium constant is defined as $K = k_f/k_b$, where k_b is the backward reaction rate coefficient.

We neglect the effects of convection in this work while including the effect of thermal fluctuations; thus, the non-equilibrium behavior of the system is modeled using Model B type diffusion-reaction equations [34, 35, 43–45, 48]. The dimensionless form of the species transport equations in this framework take the form,

$$\frac{\partial \phi_i(\mathbf{r}, t)}{\partial t} = \sum_j \nabla \cdot (M_{ij}(\{\phi_i\}) \nabla \mu_j(\{\phi_i\})) + Da_f R_i(\{\phi_i\}) + \alpha N_r^{-1/4} \theta_i(\mathbf{r}, t), \quad (1)$$

where ϕ_i denotes the volume fraction of species i , t is the dimensionless time, M_{ij} is the species mobility matrix, μ_i is the chemical potential of the i^{th} species, Da_f is the Damkohler number based on the forward reaction rate, N_r is the reference polymer length, and R_i is a dimensionless rate of generation of species i due to reaction. The last term in eqn (1) accounts for thermal noise, denoted by θ_i , and α is a factor introduced to regulate the strength of the thermal noise. We solve eqn (1) for ϕ_{Ah} , ϕ_{Ad} and ϕ_{Bd} , and assume an incompressible system to obtain $\phi_{Bh} = 1 - \phi_{Ah} - \phi_D$.

The volume fraction dependent mobility matrix is calculated using a Rouse model [34, 35, 43,

44] with the matrix elements,

$$\begin{aligned} M_{ii} &= \phi_i(1 - \phi_i), \\ M_{ij} &= -\phi_i\phi_j. \end{aligned} \quad (2)$$

The chemical potential is obtained as a functional derivative of the Helmholtz free energy with respect to the volume fraction, $\mu_i = \delta F / \delta \phi_i$. We assume an incompressible system, hence we obtain exchange chemical potentials with respect to the B homopolymer [49]. The free energy functional is obtained by perturbing the free energy as a function of concentration fluctuations about a homogeneous state using the random phase approximation [50]. The response functions obtained are approximated using their asymptotic forms, and then Fourier inverted to a weak segregation form of the free energy [51]. Finally, the free energy functional is transformed to a generalization in the strong segregation case using the procedure outlined by Uneyama and Doi [36]. The intermediate steps have been described in a previous work, which shows that for symmetric diblocks the free energy functional is given by [34],

$$\begin{aligned} F = \int d\mathbf{r} & \left[\frac{\phi_{Ah}(\mathbf{r}) \log(\phi_{Ah}(\mathbf{r}))}{N_r} + \frac{\phi_{Bh}(\mathbf{r}) \log(\phi_{Bh}(\mathbf{r}))}{N_r} \right. \\ & + 0.4015 \left(\frac{\phi_{Ad}(\mathbf{r}) \log(\phi_{Ad}(\mathbf{r}))}{2N_r} + \frac{\phi_{Bd}(\mathbf{r}) \log(\phi_{Bd}(\mathbf{r}))}{2N_r} \right) \\ & - \frac{2\sqrt{\phi_{Ad}(\mathbf{r})\phi_{Bd}(\mathbf{r})}}{2N_r} + \chi(\phi_{Ah}(\mathbf{r}) + \phi_{Ad}(\mathbf{r}))(\phi_{Bh}(\mathbf{r}) + \phi_{Bd}(\mathbf{r})) \\ & + \frac{b^2}{24} \left(\frac{|\nabla\phi_{Ah}(\mathbf{r})|^2}{\langle\phi_{Ah}\rangle} + \frac{|\nabla\phi_{Ad}(\mathbf{r})|^2}{\langle\phi_{Ad}\rangle} + \frac{|\nabla\phi_{Bd}(\mathbf{r})|^2}{\langle\phi_{Bd}\rangle} + \frac{|\nabla\phi_{Bh}(\mathbf{r})|^2}{\langle\phi_{Bh}\rangle} \right) \\ & \left. + \int d\mathbf{r}' \frac{9}{8\bar{\phi}_D N_r^2 b^2} G(\mathbf{r} - \mathbf{r}') \{(\phi_{Ad}(\mathbf{r}) - \phi_{Bd}(\mathbf{r}))\} \{(\phi_{Ad}(\mathbf{r}') - \phi_{Bd}(\mathbf{r}'))\} \right], \end{aligned} \quad (3)$$

where N_i denotes the lengths of each specie and the overbars denote spatial average volume fractions. The first four terms of the form $\phi \log(\phi)$ denote the translational entropies of the four species. The two halves of the diblock are connected, hence the next term proportional to $\sqrt{\phi_{Ad}\phi_{Bd}}$ and the factor 0.4015 corrects the overcounting of the diblock translational degrees of freedom. The term after this is the enthalpic interaction between unlike A and B segments, and the unlike halves of the diblock, with χ denoting the Flory-Huggins interaction parameter. The next four terms proportional to $|\nabla\phi_i|^2$ are square gradient terms, which penalize formation of interfaces. The last term describes the covalent bonding between the two halves of the diblock, and prevents macrophase

separation of the two blocks. The Green's function in this term satisfies $\nabla^2 G(\mathbf{r} - \mathbf{r}') = -\delta(\mathbf{r} - \mathbf{r}')$. Note that this form of the free energy functional holds only for a diblock copolymer architecture.

The two homopolymers have reactive groups at one end, and react via an end-coupling reaction, which is second order in the homopolymer concentrations. In general, the reaction can be reversible, with the backward reaction modeled as first order in the diblock concentration. The rate of generation of the species must satisfy the constraint that the total number of monomers of species A and B must remain constant. This gives [34]

$$\begin{aligned} R_{Ah} &= -R_{Ad} = -\frac{\phi_{Ah}\phi_{Bh}}{N_{Bh}} + \frac{k_b\phi_{Ad}}{k_f}, \\ R_{Bh} &= -R_{Bd} = -\frac{\phi_{Ah}\phi_{Bh}}{N_{Ah}} + \frac{k_b\phi_{Bd}}{k_f}, \end{aligned} \quad (4)$$

where k_f and k_b are the reaction rate constants of the forward and backward reactions, respectively.

The noise term in eqn (1) satisfies fluctuation-dissipation theorem (FDT) statistics [48],

$$\begin{aligned} \langle \theta_i(\mathbf{r}, t) \rangle &= 0, \\ \langle \theta_i(\mathbf{r}, t) \theta_j(\mathbf{r}', t') \rangle &= -2 \nabla \cdot [M_{ij}(\{\phi_i\}) \nabla \delta(\mathbf{r} - \mathbf{r}') \delta(t - t')]. \end{aligned} \quad (5)$$

The term α in eqn (1) is introduced to regulate the strength of the noise term. At low species concentrations, full strength fluctuations ($\alpha = 1$) can drive species compositions to negative values, which is unphysical and renders the simulations unstable because of the $\log(\phi)$ terms in the chemical potential. The factor α allows us to reduce the strength of the fluctuations, such that the simulations remain stable, and the volume fractions do not cross the $[0, 1]$ bound.

The multi-fluid model is solved numerically using a custom CUDA/C++ program [34, 35]. Time is discretized using a semi-implicit scheme, which is not as costly as fully implicit methods, yet allows larger time steps than fully explicit schemes. Space is discretized using a pseudo-spectral method with a plane wave basis that offers high accuracy in resolving spatial derivatives. We assume periodic boundary conditions and rectangular geometries.

3 Results and discussion

For this work, we consider binary homopolymer mixtures, symmetric in length and composition. The reactively formed diblock has a length twice that of the homopolymers. The equilibrium phase

diagram for such a system in the $\chi N_r - \phi_D$ space has been determined using self consistent field theory (SCFT) [34], and is shown in Fig. 1. The system can be in a disordered phase (DIS), a lamellar phase (LAM), macroscopically segregated into two phases (2ϕ), or be in a three phase coexistence (3ϕ) with homopolymer macrophases and a diblock LAM interphase swollen with the homopolymers. Note that the free energy functional used in the present phase-field model is an approximation of the functional used in SCFT to generate the phase diagram, hence the phase boundaries will differ in detail. Nevertheless, the equilibrium phase on complete conversion of the homopolymers to diblock obtained from the phase-field model, as well as the intermediate phases observed as the reaction progresses is consistent with the prediction from SCFT. This consistency between the phase-field simulations and SCFT has been demonstrated previously [34].

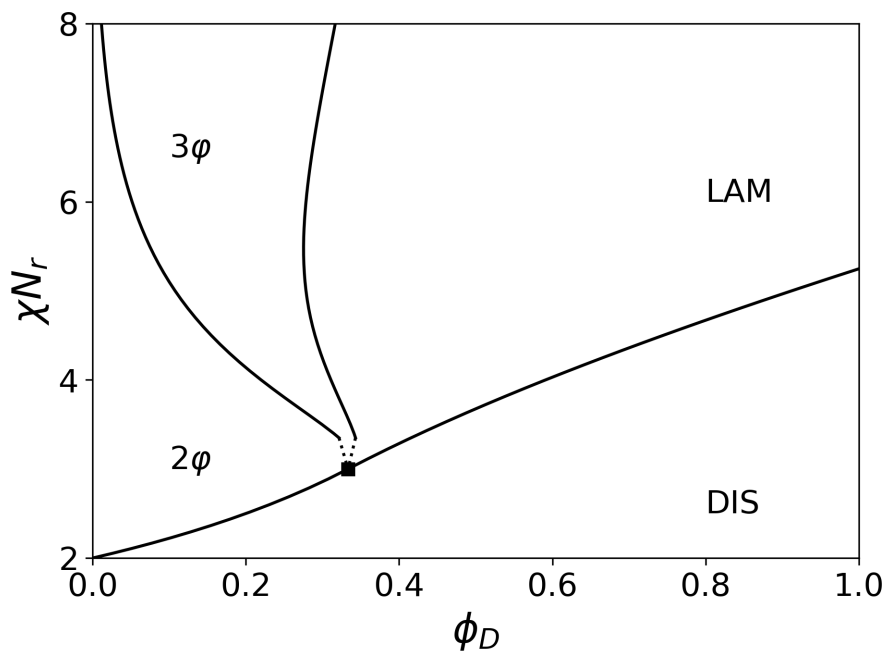


Figure 1: Phase diagram in the $\chi N_r - \phi_D$ plane for a blend of homopolymers symmetric in length and composition, where the length of the diblock is twice the length of the homopolymer.

In the following subsections, we discuss the effects of different parameters on diffusion-reaction phenomena, including interfacial roughening and spontaneous emulsification.

3.1 Initial distribution of homopolymers

We will focus our attention on 2-D systems, having initially macroscopically segregated homopolymers, as shown in Fig. 2. This distribution corresponds to a film of homopolymer A cast on top of a film of homopolymer B. Such geometries have been studied extensively in experiments [5–9]. The two homopolymers have a uniform concentration along the length of the film. Thus, there is no concentration gradient along the length of the simulation box, L_x . The thickness of the film, or the homopolymer layers is set by the width of the box, L_y . The initial concentration profile across the width of the box is shown in Fig. 2(b). With periodic boundary conditions, the initial distribution is symmetric about the center of the box, thus there are two interfaces in the y direction. In all the simulations, the initial diblock concentration is set to be uniform at $\phi_{D_0} = 0.02$. This numerically small value is used to avoid singular thermodynamic forces resulting from vanishing amounts of any of the species. Fig. 2(a) shows a flat interface between the homopolymers, however in experiments, thermal fluctuations will cause perturbations at the interface. Hence, the initial flat interface is seeded with random noise of magnitude $|\delta\phi| = 0.001$ about the average composition of each species. Note that the fluctuations are only added to the initial concentration profiles of the species, and the simulations discussed in the following subsections do not include thermal fluctuations (i.e., $\alpha = 0$). The effect of thermal fluctuations is considered at the end of this section.

In addition to the flat interface seeded with random noise, we have investigated the morphology evolution of interfaces that are initially perturbed by sinusoids having a wavelength equal to L_x , and $L_x/3$. These initial distributions will be referred to as long wavelength and short wavelength, respectively, henceforth. We also study a fourth initial configuration corresponding to a zig-zag interface between the homopolymers. The concentration profiles of homopolymer A, ϕ_{Ah} corresponding to these four different initial distributions are depicted in Fig. 3 under the panel corresponding to $t = 0$. The subsequent panels in Fig. 3 show snapshots of the concentration profile of the A block of the diblock, ϕ_{Ad} , at different times after the start of the simulation. The simulations for all the different initial distributions were performed for an irreversible reaction with $Da_f = 1$, $\chi N_r = 7$ and a box size $(L_x, L_y) = (32, 16)$. The homopolymers react and produce diblock at the interface. Over time, the diblock concentration at the interface builds up, resulting in compatibilization of the homopolymers, and the interface broadens. The interfacial reaction is

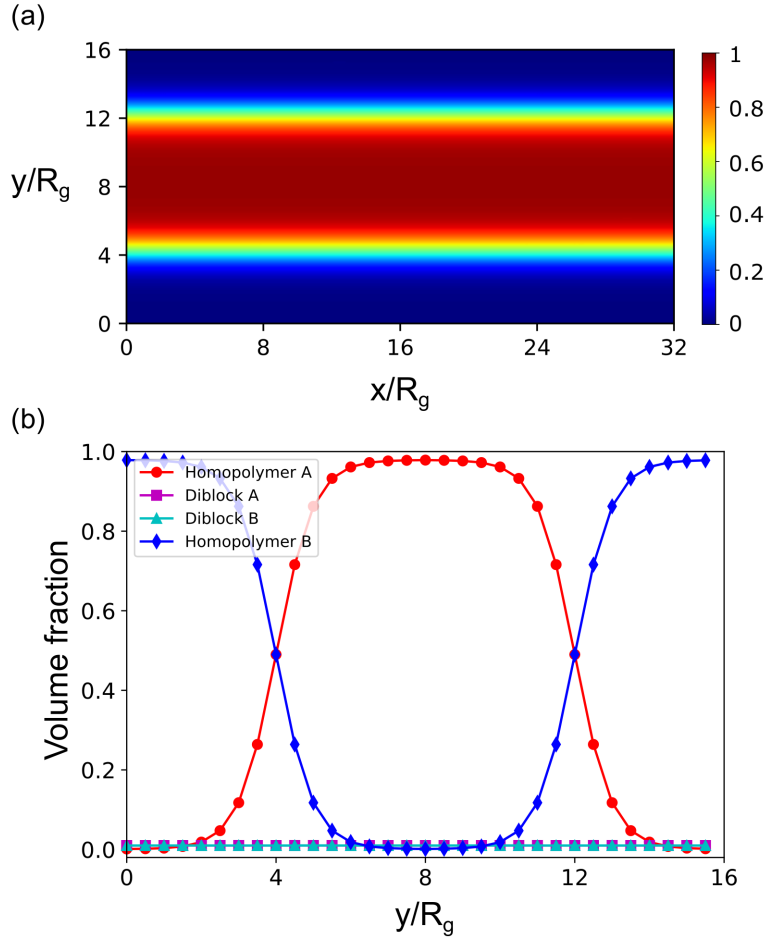


Figure 2: Representation of the initial distribution between the homopolymers, corresponding to macroscopically segregated homopolymers. (a) 2-D concentration profile of homopolymer A (ϕ_{Ah}). The interface between the homopolymers is seeded with random noise of magnitude $|\delta\phi| = 0.001$ about the average composition. (b) 1-D concentration profile of all species obtained by taking a slice from (a) at $x = 16R_g$, showing the gradient in species concentrations.

accompanied by the diffusion of diblock from the interface to the bulk homopolymers, and of the homopolymers from the bulk to the interface due to chemical potential gradients. The build-up of the diblock copolymer at the interface reduces the interfacial area available for reaction, thus the reaction slows down. When sufficient diblock is formed, the interface starts developing undulations and begins to roughen. We denote the time at which this occurs as the roughening time, t_r . The concentration profile of the A block of the diblock, ϕ_{Ad} at the onset of roughening is shown in Fig. 3, under the panel $t = t_r$. The roughening of the interface increases the interfacial area

available for reaction, and the reaction rate increases slightly at this point. Subsequently, sufficient diblock diffuses into the bulk domains, and leads to the formation of domains of homopolymer B-swollen drops of the B half of the diblock in a matrix of homopolymer A and the A half of the diblock; and another domain of homopolymer A-swollen drops of the A half of the diblock in a matrix of homopolymer B and the B half of the diblock. The snapshot of the ϕ_{Ad} profile at such a time is shown in the panel under $t = 65$ of Fig. 3. This intermediate morphology is reminiscent of spontaneous emulsification observed in several experimental studies [5–9], although the simulation domain employed here covers a fraction of the area in the TEM images typically captured. Eventually, these drops coalesce, and form a lamellar phase phase, as shown in the last panel of Fig. 3.

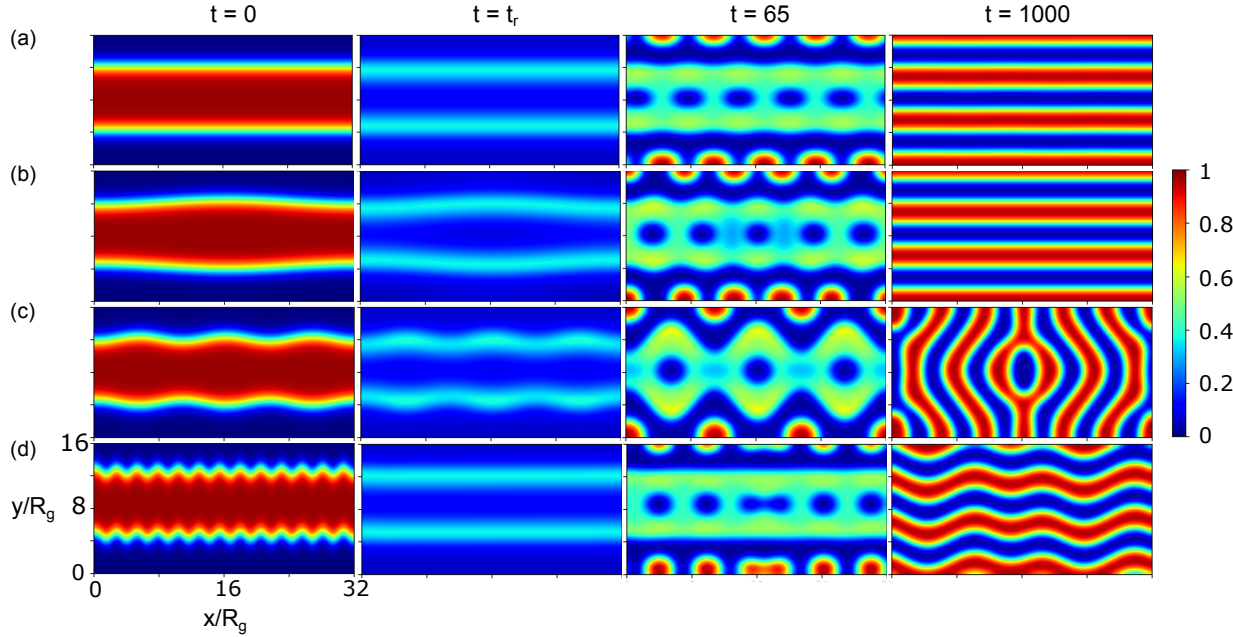


Figure 3: Snapshots of the concentration profile corresponding to an initial distribution between the homopolymers having a (a) flat interface seeded with noise (flat), (b) sinusoid perturbed interface with wavelength equal to the box length, L_x (long), (c) sinusoid perturbed interface with wavelength equal to $L_x/3$ (short), and (d) a zig-zag interface (zig-zag). The initial profile at $t = 0$ corresponds to the concentration of homopolymer A, ϕ_{Ah} , and the subsequent profiles correspond to the concentration of the A half of the diblock, ϕ_{Ad} . For all the simulations, $Da_f = 1$, $\chi N_r = 7$, and the box size was held fixed at $(L_x, L_y) = (32, 16)$.

The visualization of the qualitative evolution of morphology is shown in Fig. 3. We now proceed to track the evolution of the system quantitatively. The reaction dynamics of the system is quantified by measuring either the reaction rate, which is the rate of generation of the diblock $\langle \dot{\phi}_D \rangle$, or the mean diblock concentration, $\langle \phi_D \rangle$, where the angular brackets represent volume averages at a specific time. The evolution of $\langle \dot{\phi}_D \rangle$ and $\langle \phi_D \rangle$ for the various initial interface configurations is shown in Figs. 4(a) and (b), respectively. The initial interfacial area of the zig-zag interface is greater than the short and long wavelength, and the flat interface has the least initial interfacial area. Therefore, the initial reaction rate of the zig-zag interface is greater than the other distributions. However, the difference in the interfacial area is not substantial enough to result in a marked difference in the subsequent reaction rate. In fact, as shown in the second column of Fig. 3, the concentration gradients along the zig-zag interface are soon eliminated, and the resulting profile is analogous to a flat interface. The build-up of diblock at the interface decreases the reaction rate monotonically, until the interface roughens. The reaction rate increases slightly, soon after the undulations caused by the roughening grow. It is clear from Fig. 4(a) and (b) that the reaction dynamics is not influenced strongly by the initial distribution of the interface. All the interfaces roughen at the same time, as evidenced by the small peak in the reaction rate at $t = 42$.

The onset of interfacial roughening, and the characteristic length scale of the morphology can be quantified by calculating the first moment of the normalized structure factor [35, 52, 53],

$$q_{Ah} = \frac{\sum_q q s_p(q, t)}{\sum_q s_p(q, t)}, \quad (6)$$

where the structure factor,

$$s_p(q, t) = \frac{1}{\int d\Omega} \int d\Omega \mathcal{F} \left[\frac{g_p(\mathbf{r}, t)}{g_p(0, t)} \right] \quad (7)$$

is given by the Fourier transform of the correlation function of the homopolymer A concentration,

$$g_p(\mathbf{r}, t) = \left\langle \int d\mathbf{r}' [\phi_{Ah}(\mathbf{r} + \mathbf{r}', t) \phi_{Ah}(\mathbf{r}', t) - \langle \phi_{Ah}(t) \rangle^2] \right\rangle, \quad (8)$$

averaged over solid angles $d\Omega$ of \mathbf{q} with $\mathbf{q} = |q|$. A characteristic domain size is then defined by $2\pi/q_{Ah}$, and its evolution is depicted in Fig. 4(c). The initial domain size corresponds to the thickness of the homopolymer A layer. At initial stages of the reaction, the diblock is generated at the interface. This results in compatibilization of the homopolymers, and the interface thickens. Thus, the characteristic domain size shows a slight increase at early time. This parameter increases

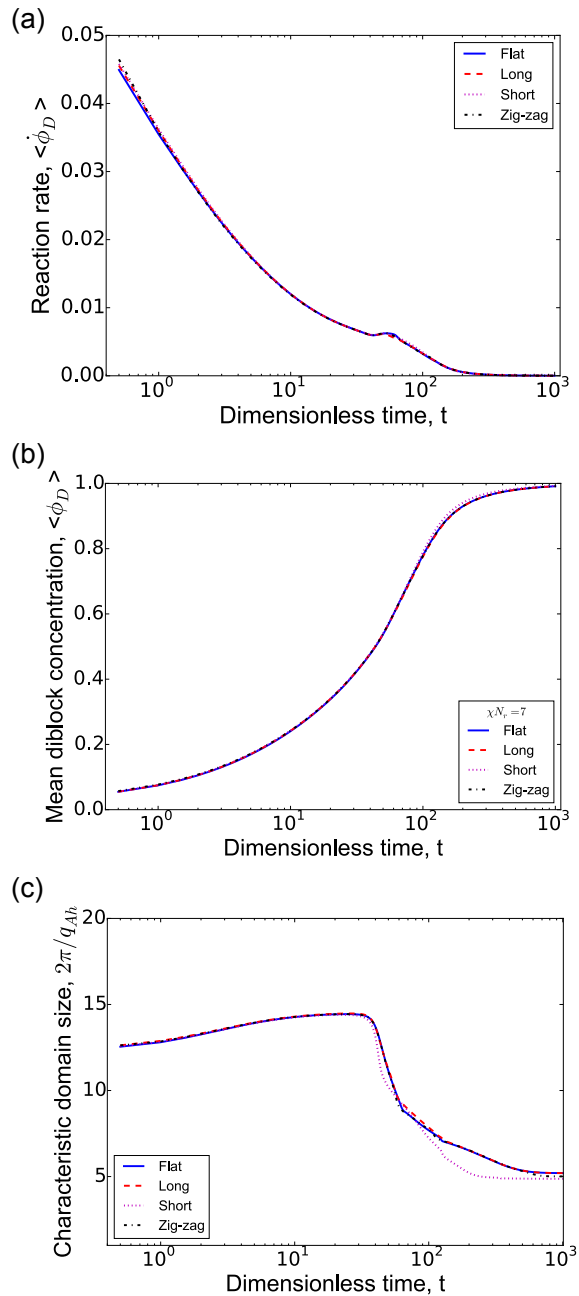


Figure 4: Temporal evolution of (a) reaction rate, (b) mean diblock concentration, and (c) characteristic domain size as a function of the initial distribution between the homopolymers. For all the simulations, $Da_f = 1$, $\chi N_r = 7$, and the box size was held fixed at $(L_x, L_y) = (32, 16)$.

until the onset of interfacial roughening, reaches a maximum value, and then starts decreasing rapidly. The morphology at this stage is depicted by the third panel of Fig. 3, where droplets of homopolymer-swollen diblock emerge. Eventually, the system relaxes to a lamellar phase and the

characteristic domain size at this time represents the lamellar spacing between the two blocks of the diblock. Similar to the evolution of the reaction dynamics, the characteristic domain size of the different initial distributions nearly overlap, suggesting that the morphology evolution is not strongly influenced by the initial interfacial distribution. The characteristic domain size for all four distributions attain the maximum value around the same time, verifying that the interfaces roughen in near concert. For subsequent systems, the time where the characteristic domain size reaches the maximum value will be used to quantify the onset of roughening.

3.2 Film thickness effects

It has been observed in experiments that thicker homopolymer domains roughen slower than thinner domains, and roughening occurs rapidly for films below a certain thickness [7, 26–28]. Hence we investigated the effect of homopolymer film thickness on the reaction dynamics and the onset of interfacial roughening by changing the size of the simulation box. Fig. 5 shows snapshots of the ϕ_{Ad} profile after the interface has roughened. For these simulations, $Da_f = 0.1$, $\chi N_r = 7$, and the initial distribution between the homopolymers is a flat interface seeded with random noise. Each row of Fig. 5 corresponds to films having the same thickness (L_y), and the length of the film increases along the row. The concentration profiles for the boxes with $L_y = 16$ correspond to $t = 500$, the boxes with $L_y = 32$ correspond to $t = 1000$, and the widest boxes with $L_y = 64$ correspond to $t = 1758$. The morphology of the films having the same thickness is similar, and is not significantly influenced by the length of the film. The intermediate morphology changes with the film thickness. For films with $L_y = 16$, the interface roughens after sufficient build-up of diblock, and the system shows spontaneous emulsification with drops of homopolymer swollen diblock appearing in a matrix of the other homopolymer, as shown in Fig. 3. For thicker films, homopolymer swollen diblock lamellae are observed to diffuse from the initial interface after sufficient diblock is generated. This decreases the thickness of the original film, and also results in the formation of new interfaces where reaction occurs. The number of lamellae diffusing out from the original interface increases with the thickness of the film, as shown by Fig. 5(b) and (c). Subsequently the film undergoes a similar instability as the film with $L_y = 16$, and homopolymer swollen diblock drops appear in the bulk which coalesce to form a lamellar phase.

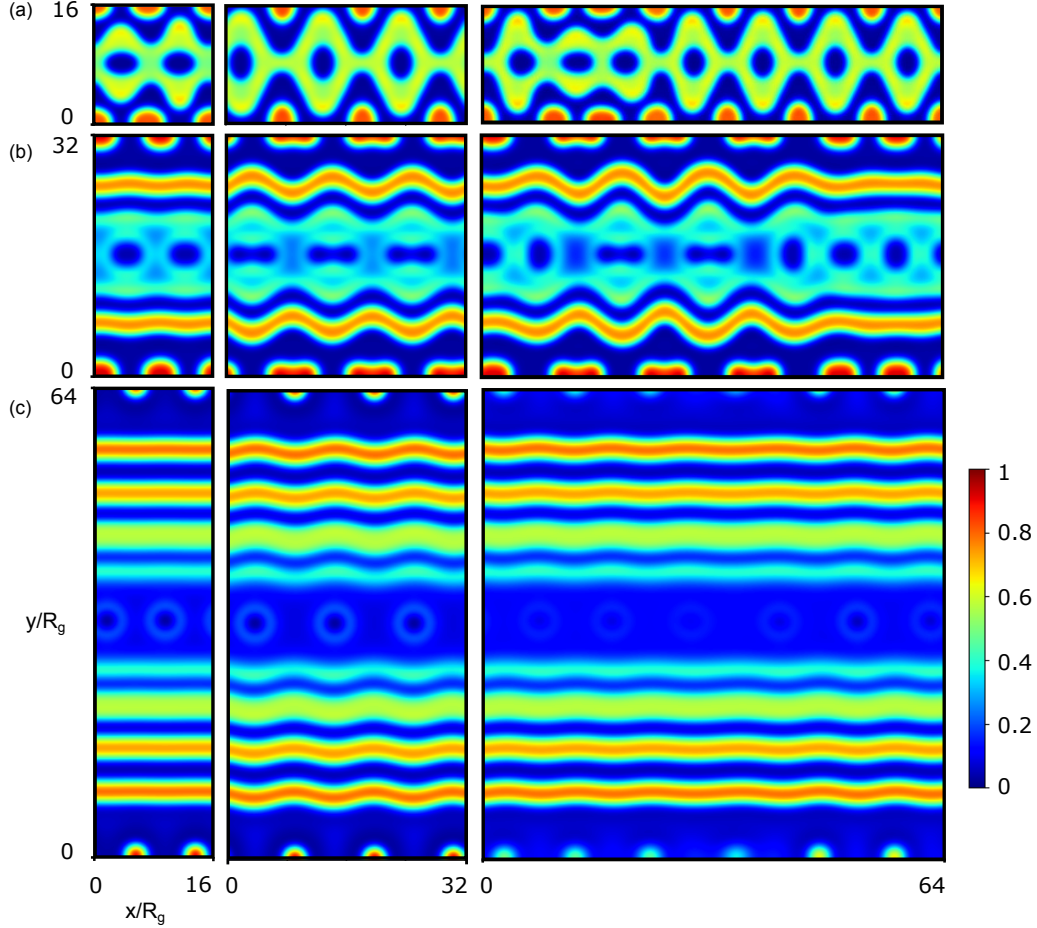


Figure 5: 2-D profiles of ϕ_{Ad} for (a) $L_y = 16$ at $t = 500$, (b) $L_y = 32$ at $t = 1000$, and (c) $L_y = 64$ at $t = 1758$. The box length, L_x increases from left to right for each row. For all the simulations, $Da_f = 0.1$, $\chi N_r = 7$, and the initial distribution between the homopolymers is a flat interface seeded with random noise.

The time at which the concentration profiles are depicted in Fig. 5 hints that the reaction dynamics and onset of roughening is slower for thicker films. This is shown quantitatively in Figs. 6 and 7. Fig. 6(a) shows the evolution of $\langle \phi_D \rangle$ for different box sizes. The data overlap for films having the same thickness but different lengths. The mean diblock concentration is less at a given time for thicker films, implying that the reaction dynamics is dictated by the thickness of the films. The homopolymers have to diffuse from the bulk through larger distances in thicker films, hence, the rate of reaction is slower for thicker films. The time scale for diffusion of the homopolymer across the film thickness, L_d is $\tau_d = L_d^2/D$, where L_d is calculated from the characteristic domain

size of homopolymer A, $2\pi/q_{Ah}$ at the start of the simulation. The evolution of mean diblock for films of different thicknesses does not collapse when the time axis is rescaled by L_d^2 , but the data can be approximately collapsed by rescaling the time axis in Fig. 6(a) with L_d , as is shown in Fig. 6(b). Thus, the diffusion length is proportional to the product of the film thickness and another length scale which is constant in all the simulations. For $Da_f = 0.1$, the system is mixed reaction-diffusion controlled. Hence, two length scales govern the process - the film thickness, L_d and the distance between the reactive ends, R_g . Rescaling the time axis by L_d is equivalent to rescaling time by the geometric mean of τ_d and the Rouse time τ_R . This suggests that the diffusion of the homopolymers through thicker domains slows the reaction for thicker films at $Da_f = 0.1$.

The evolution of the morphology is quantified by plotting the characteristic domain size for the films with different thickness in Fig. 7. The film with $L_y = 16$ has one maxima corresponding to the roughening of the interface (Fig. 7(a)). The concentration profiles in the right correspond to the snapshots at time instances marked in the plot, and show the ϕ_{Ad} profile at the onset of roughening, after emulsification, and the final morphology. The characteristic domain size for thicker films starts to decrease sharply after attaining a maximum value, but there are multiple instances where the domain size shows a sudden decrease, as shown in Fig. 7(b) and (c). The thickness of the interface increases initially with diblock formation, which results in an increase in the characteristic domain size. Homopolymer-swollen diblock lamellae diffuse from the interface of the original film upon build-up of sufficient diblock. The earlier points of sudden decay correspond to the lamellae diffusing from the original interface, which decreases the domain size. For these films, the final such point corresponds to an instability analogous to the film with $L_y = 16R_g$, leading to the spontaneous formation of an emulsion. For all films, the onset of roughening is determined by tracking the first instance of rapid decay, which is the maximum value of the characteristic domain size. This point is chosen because the original interface ceases to exist beyond this point.

3.3 Reaction kinetics

We quantify the effect of reaction kinetics by the Damkohler number, Da_f . The effect of Da_f on the reaction dynamics and the onset of roughening is shown in Fig. 8. For these simulations, $\chi N_r = 7$, $(L_x, L_y) = (32, 16)$, the initial distribution between the homopolymers is a flat interface

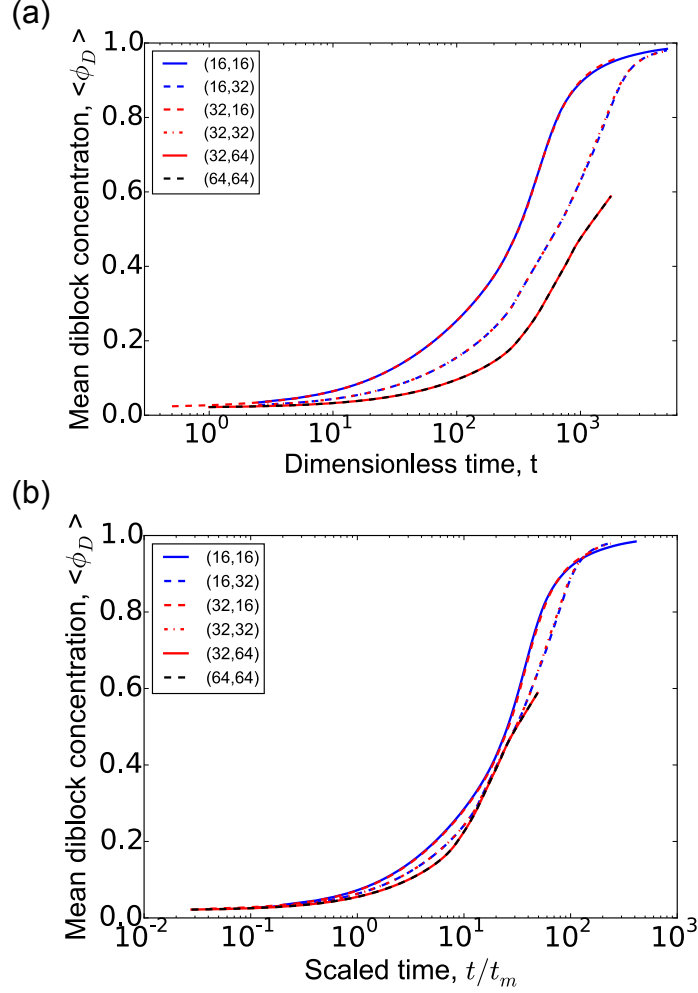


Figure 6: Evolution of the mean diblock concentration as a function of box size with (a) dimensionless time, and (b) time rescaled by t_m , the geometric mean of the diffusion time ($\tau_d = L_d^2/D$) and the Rouse time ($\tau_R = R_g^2/D$). Here, $Da_f = 0.1$, $\chi N_r = 7$, and the initial distribution between the homopolymers is a flat interface seeded with random noise.

seeded with random noise, and the reactions are assumed to be irreversible. The reaction rate increases as Da_f increases, as is shown by Fig. 8(a). For $Da_f = 1$, the reaction is nearly complete at $t = 1000$, while the corresponding conversion of the diblock at the same time for $Da_f = 0.01$ is 25%. For irreversible reactions, Da_f is a relative measure of the diffusion and reaction time scales. The reaction time scale is faster at higher Da_f , resulting in faster reaction dynamics.

The time at which the interface roughens, or the roughening time, t_r , is determined from the maxima in the characteristic domain size shown in Fig. 8(b). The variation of t_r with Da_f for

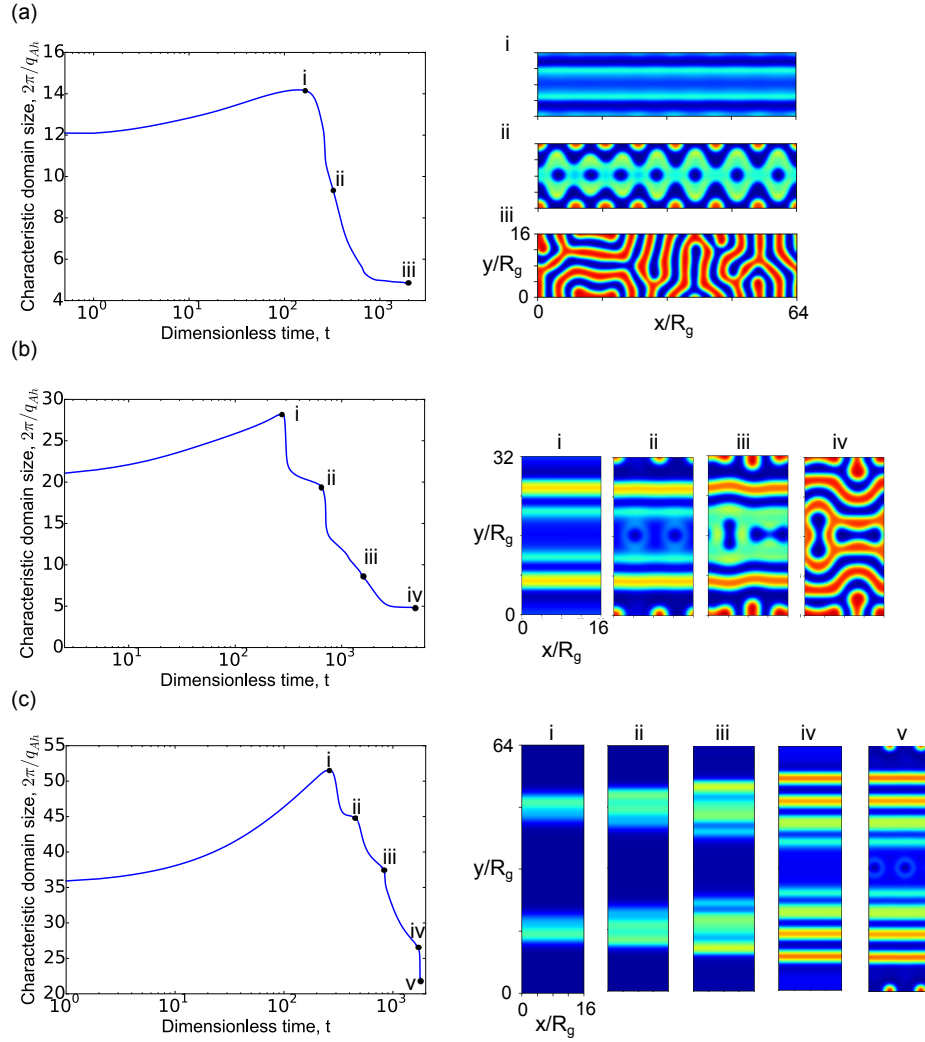


Figure 7: Temporal evolution of the characteristic domain size for (a) $L_y = 16$, (b) $L_y = 32$, and (c) $L_y = 64$. The snapshots correspond to the profile of ϕ_{Ad} at different time instances marked in the plot. Here, $Da_f = 0.1$, $\chi N_r = 7$, and the initial distribution between the homopolymers is a flat interface seeded with random noise.

films of different lengths and thicknesses at $\chi N_r = 7$ is depicted in Fig. 9. For a given film, t_r decreases nearly inversely with Da_f ; hence, the interface roughens faster as Da_f increases. Films with the same thickness roughen approximately at the same time, regardless of the length of the film. For the three films studied, the thinnest film roughens faster than the thicker films. This is in agreement with experimental findings that thinner films are more prone to roughening and spontaneous emulsification [7, 26, 27]. For both the thicker films, t_r is nearly the same,

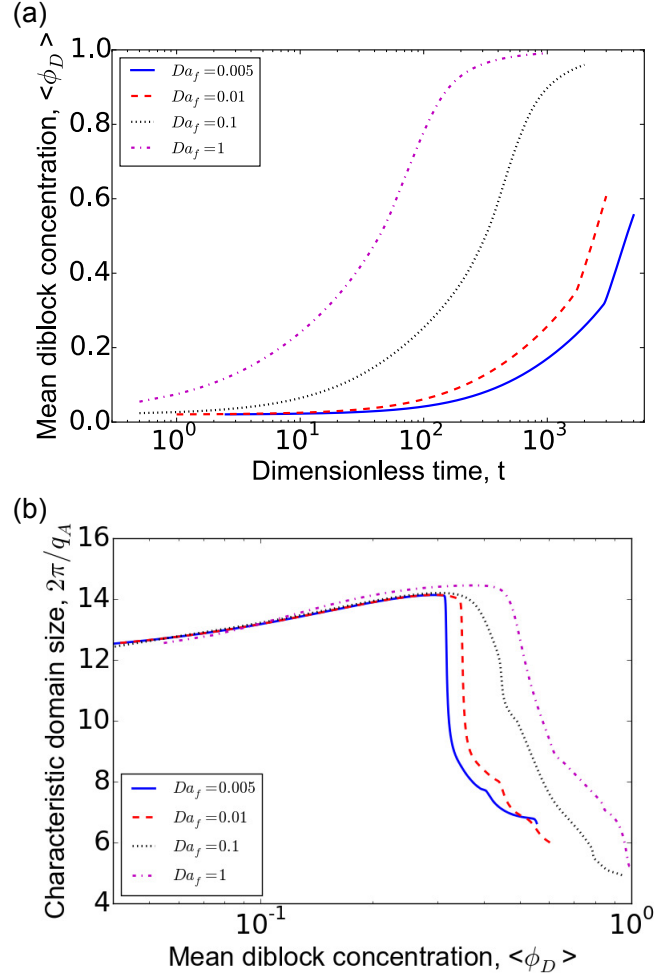


Figure 8: (a) Temporal evolution of mean diblock concentration, and (b) evolution of the characteristic domain size as a function of $\langle \phi_D \rangle$ for different Da_f . For all the simulations, $\chi N_r = 7$, $(L_x, L_y) = (32, 16)$, and the initial distribution between the homopolymers is a flat interface seeded with random noise.

and corresponds to the diffusion of homopolymer swollen lamellae from the interface to the bulk homopolymer domains, as depicted by the insets (i) in Fig. 7(b) and (c). The original interface becomes ill-defined beyond this point. Although t_r calculated using this procedure is the same for $L_y = 32$ and $L_y = 64$, the corrugation of the interface, and emulsification is faster for the film with $L_y = 32$, as seen in the insets of Fig. 7(b) and (c).

The onset of roughening has previously been attributed to the interfacial excess diblock, z^* reaching a critical value where the interfacial tension becomes vanishingly small. The interfacial

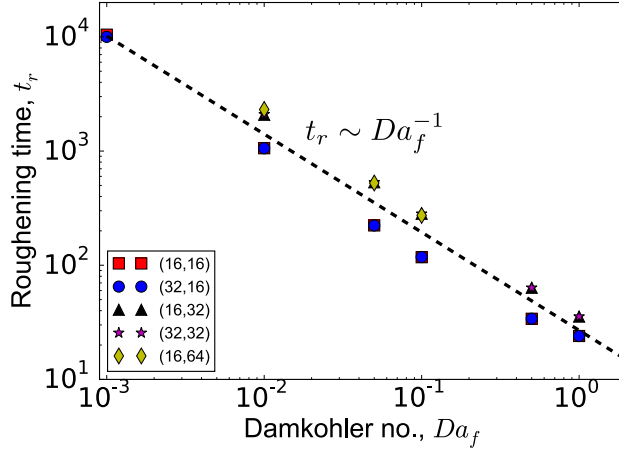


Figure 9: Roughening time as a function of Da_f and box size. For all the simulations, $\chi N_r = 7$, and the initial distribution between the homopolymers is a flat interface seeded with random noise.

excess diblock is calculated experimentally using forward recoil spectrometry (FRES), and the interfacial tension is then determined from mean field theories developed for flat interfaces using the experimentally measured values of z^* [4–6, 8]. Here, we calculate the surface excess number of the diblock as $n_D^{(s)} = n_D^{(tot)} - n_D^A - n_D^B$, where n_D is the number of diblock species, and the superscripts denote the surface, total volume, bulk homopolymer A, and bulk homopolymer B phases, respectively [54]. With Fig. 2 as reference, the bulk homopolymer B region is located at $y = 0$, and the bulk homopolymer A region is located at $y = 8$, or more generally, at $y = L_y/2$. The calculation of $n_D^{(s)}$ involves determining the location of the interface. The species concentration gradients are across the thickness of the film. Hence, the interface is located by determining the location along the width of the box where there is no surface excess of non surface-active species, i.e., either of the homopolymers. This is equivalent to determining the Gibbs dividing surface [55]. The number of species, n_i , can be calculated from the mean volume fraction of the species as $n_i = \frac{\bar{\phi}_i V}{N_i v_0}$, where V is the system volume, v_0 is the monomer volume and N_i is the length of the species. Using this definition for homopolymer A, the interface is located at

$$y_I = \left(\frac{\bar{\phi}_{Ah}^A - \bar{\phi}_{Ah}^B}{\bar{\phi}_{Ah}^A - \bar{\phi}_{Ah}^B} \right) \frac{L_y}{2}. \quad (9)$$

Here, $\bar{\phi}_{Ah}$ is the mean concentration of homopolymer A in half the box, $\bar{\phi}_{Ah}^A = \int \phi_{Ah}|_{y=L_y/2} dx/L_x$ is the mean homopolymer A concentration in the bulk homopolymer A phase, and $\bar{\phi}_{Ah}^B = \int \phi_{Ah}|_{y=0} dx/L_x$ is the mean homopolymer A concentration in the bulk homopolymer B phase. The interfacial

excess areal density of the diblock is then determined from $z^* = n_D^{(s)} N_D v_0 / A$, where A is the cross-sectional area of the interface. We get

$$z^* = \frac{L_y}{2} \bar{\phi}_D - y_I \bar{\phi}_D^B - \left(\frac{L_y}{2} - y_I \right) \bar{\phi}_D^A. \quad (10)$$

Here $\bar{\phi}_D^A$ and $\bar{\phi}_D^B$ denote the concentration of the diblock in the bulk A and B homopolymer domains, respectively. Although z^* grows with the system size, it is, in a thermodynamic sense, the number of diblock at the interface per unit area, multiplied by a constant (the chain volume).

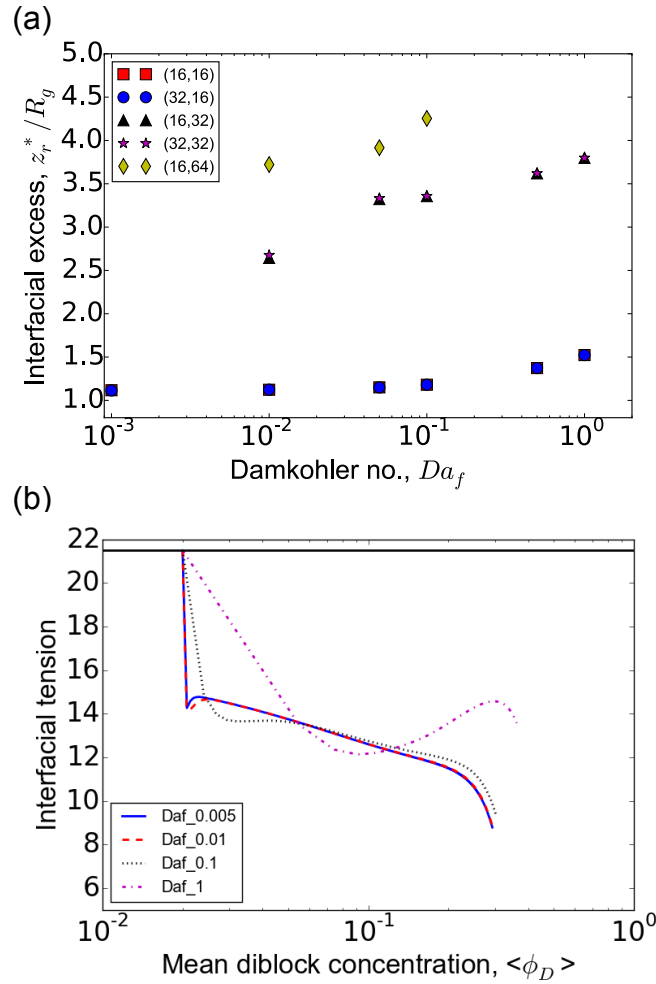


Figure 10: (a) Interfacial excess diblock concentration at the onset of roughening as a function of Da_f and box size, for $\chi N_r = 7$. (b) Interfacial tension up to the onset of roughening plotted against the mean diblock concentration, $\langle \phi_D \rangle$ as a function of Da_f for $\chi N_r = 7$ and $(L_x, L_y) = (32, 16)$. The initial distribution between the homopolymers is a flat interface seeded with random noise.

The interfacial excess diblock is calculated up to the onset of roughening because the interface becomes ill-defined once roughening and spontaneous emulsification starts. Fig. 10(a) shows the interfacial excess diblock at the onset of roughening as a function of Da_f , and for different film geometries. For reaction kinetics limited systems, quantified by small values of Da_f (< 0.1), z^*/R_g approaches a limiting value. In these systems, the reaction is inherently slow, and the diblock is continuously generated at the interface until the interface roughens. At higher Da_f , the kinetics is faster, and buildup of diblock at the interface is faster, leading to an earlier onset of roughening. Although the simulations in Fig. 10 are for a flat initial interface between the homopolymers, the roughening time and interfacial excess diblock at the onset of roughening are nearly the same for the other initial distributions studied. These have not been shown to avoid crowding the figure.

Similar to the interfacial excess, the interfacial tension becomes an ill-defined quantity when the interface roughens. There has been discrepancy in previous computational studies regarding the value of the interfacial tension at the onset of roughening. Studies using MD simulations, as well as DPD simulations, calculated the interfacial tension as the difference between the normal and tangential components of the pressure tensor across the interface. The MD simulations concluded that the interfacial tension drops to negative values and was the reason for the roughening, while the DPD simulations did not observe significant reduction of the interfacial tension at roughening [29–32]. We determine the interfacial tension from the excess Helmholtz free energy, $F^{(s)}$, with the constraint that the surface excess of non surface-active species is zero [54, 55]. The surface excess grand potential, σA , is given by

$$\sigma A = F^{(s)} - \mu_D n_D^{(s)}, \quad (11)$$

where σ is the interfacial tension, and μ_D is the chemical potential of the diblock, obtained as the functional derivative of the free energy functional in eqn (3). The surface excess Helmholtz free energy is also obtained from eqn (3) by subtracting the local free energy of the bulk homopolymer phases from the total free energy of the system. The evolution of interfacial tension until the onset of roughening is shown in Fig. 9(b). The black line shows the interfacial tension at $t = 0$. Initially, as the reaction starts and copolymer is generated at the interface, the interfacial tension decreases. The copolymer layer compatibilizes the blend and entrains the homopolymers, resulting in the

broadening of the interface. The copolymer is formed and distributed in the diffuse interface. This dilutes the concentration of the copolymer at the location of the interface (eqn (9)), and the interfacial tension slightly increases at this point. As more copolymer is formed, the dilution effect is overcome, and the interfacial tension begins to decrease rapidly until the interface roughens. Although the interfacial tension drops sharply before roughening, it does not approach vanishingly small or negative values. Thus, we conclude that a negative interfacial tension is not a prerequisite to the roughening of reacting interfaces. A similar conclusion was obtained from studies using DPD simulations [30, 31].

3.4 Reversible reactions and fraction of reactive homopolymers

The faster onset of roughening for systems with higher Da_f suggests that there is possibly a critical interfacial excess diblock, or a critical mean diblock concentration for the phenomenon. To determine if such a critical value exists, we perform one set of simulations with reversible reactions, and another set of reactions where a only fraction of the homopolymers have a reactive end group. This allows us to control the final diblock concentration and interfacial excess diblock in the system.

Fig. 11(a) and (b) quantifies the reaction dynamics and characteristic domain size for systems with reversible reactions, which is characterized by the equilibrium constant, K . For all the simulations, $Da_f = 1$, $\chi N_r = 7$, $(L_x, L_y) = (32, 16)$, and the initial distribution between the homopolymers is perturbed by a long wavelength sinusoid. The dynamics of the irreversible reaction is also shown for comparison. The equilibrium diblock concentration increases with K because the rate constant for the backward reaction decreases relative to k_f upon increasing K . The systems with $K/N_r = 2$ and 10 do not show a sudden decrease in the evolution of the characteristic domain size. This parameter approaches a constant value as the reaction proceeds to equilibrium for $K/N_r = 2$ and 10. Nor do these systems show interfacial roughening and spontaneous emulsification. The equilibrium for these systems corresponds to a 2φ state with the diblock sandwiched between the segregated homopolymers, as shown by the 1-D concentration profile at $x = 16$ for $K/N_r = 10$, in the inset of Fig. 12(a).

An alternate method to control the final concentration of the diblock in the system is to pre-

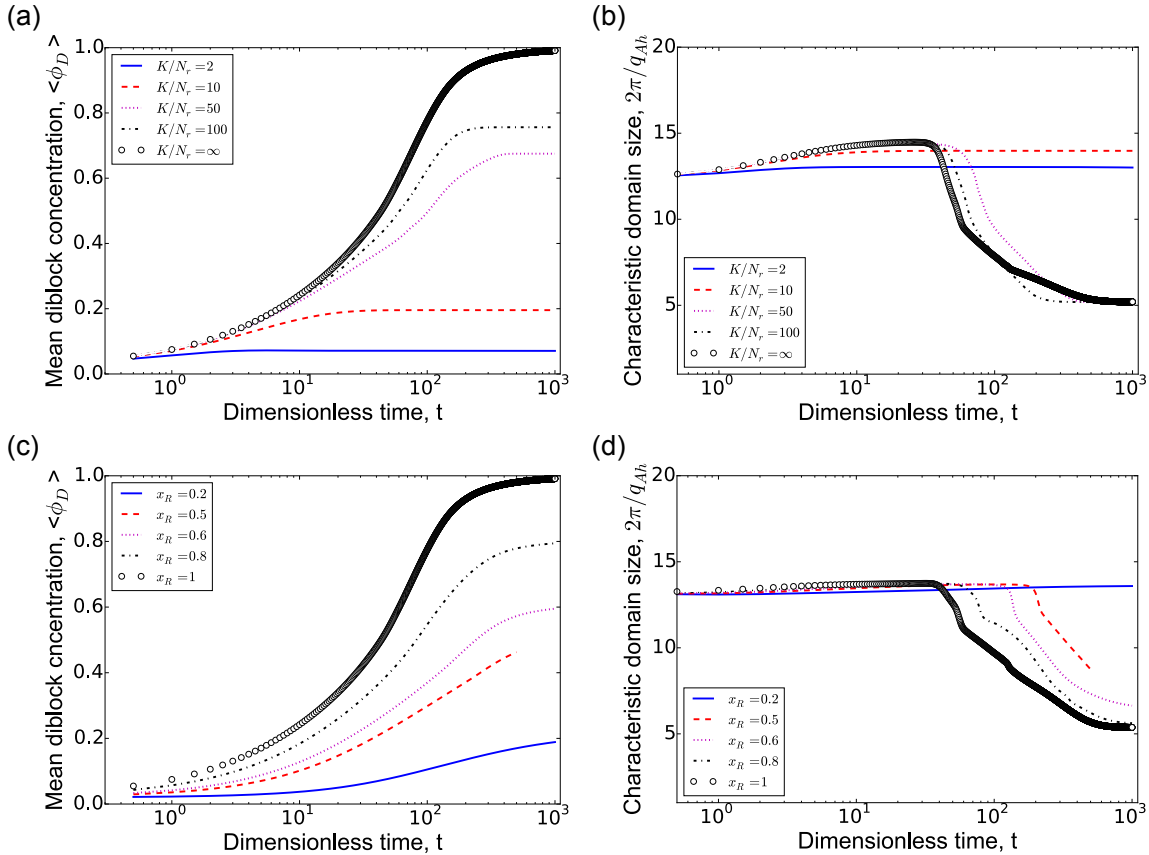


Figure 11: Temporal evolution of (a) mean diblock concentration, and (b) characteristic domain size as a function of K/N_r . Temporal evolution of (c) mean diblock concentration, and (d) characteristic domain size as a function of the fraction of homopolymers with a reactive end group, x_R . For all the simulations, $Da_f = 1$, $\chi N_r = 7$, $(L_x, L_y) = (32, 16)$, and the initial distribution between the homopolymers is perturbed by a long wavelength sinusoid.

scribe the fraction of homopolymers, x_R , that have a reactive end group. Such systems are modeled by introducing two more species to describe the non-reactive homopolymers, and writing two additional transport equations. These species contribute to the translational entropy and enthalpy terms in the free energy functional, and are straightforward to implement. The results for varying x_R on the reaction dynamics and characteristic domain size are shown in Fig. 11(c) and (d), and the system where all the homopolymers have reactive end groups ($x_R = 1$) is also shown for comparison. The final diblock concentration increases with x_R because of the availability of more reactants. Systems where a small fraction of homopolymers are reactive do not undergo roughen-

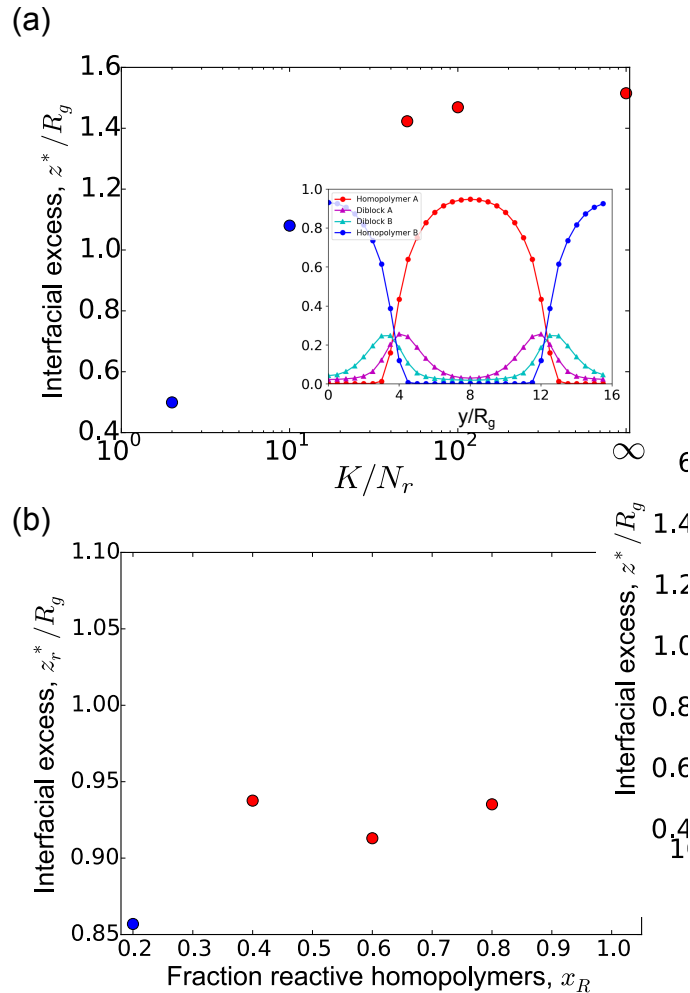


Figure 12: Interfacial excess diblock concentration at the onset of roughening (red), or at the end of the simulation (blue) as a function of (a) K/N_r , and (b) x_R . The inset in (a) shows the 1-D concentration profile at equilibrium for $K/N_r = 10$ at $x = 16R_g$. For all the simulations, $Da_f = 1$, $\chi N_r = 7$, $(L_x, L_y) = (32, 16)$, and the initial distribution between the homopolymers is perturbed by a long wavelength sinusoid.

ing, as shown by the evolution of the characteristic domain for the system with $x_R = 0.2$. The final state at $x_R = 0.2$ corresponds to a 2φ system.

The interfacial excess diblock for systems with reversible reactions, and with a fraction of reactive homopolymers is shown in Fig. 12(a) and (b), respectively. For systems that do not show roughening, the interfacial excess at the end of the simulation is plotted by the blue circles, and for systems that undergo roughening and spontaneous emulsification, the interfacial excess at the

onset of roughening is depicted by the red circles. The plots seem to suggest that there might not be a critical interfacial excess diblock concentration at which roughening occurs. At equilibrium, $z^*/R_g = 1.09$ for the system with $K/N_r = 10$, which is greater than z^*/R_g at the onset of roughening for the systems with a fraction of reactive homopolymers. Comparing the final $\langle\phi_D\rangle$ to the equilibrium phase diagram of this ternary system obtained from SCFT (Fig. 1), it appears that systems with a diblock concentration greater than the concentration around the phase boundary between the 3φ and lamellar phase are observed to undergo roughening. However, it should be noted that the free energy functional used in our phase-field model is an approximation to the functional used to generate the equilibrium phase diagram in Fig. 1; hence, the phase boundaries for our model will be somewhat different. For example, at the equilibrium diblock concentration for $K/N_r = 10$, SCFT predicts that the system is in a 3φ state, whereas the inset in Fig. 12(a) shows a 2φ state. Nonetheless, a critical amount of diblock must be formed to drive interfacial roughening. This suggests that roughening occurs when sufficient copolymer is formed to induce microphase separation to a lamellar microstructure. This, again, supports the conclusion of studies using DPD simulations [30, 31].

3.5 Thermal fluctuations

Several studies have hypothesized that thermal fluctuations accelerate the onset of interfacial roughening [7, 9]. As previously mentioned, the $\log(\phi)$ terms in the free energy functional cause the simulations to become unstable when full strength thermal fluctuations are incorporated. Here, we study the effect of weak thermal fluctuations on the evolution of the system, and summarize the results in Fig. 13. The system is initialized with nearly pure homopolymers, hence the concentration of the diblock is extremely small at early times. As the reaction proceeds, the reactants are consumed, and at late times, the homopolymers are nearly exhausted. Thus, the concentration of some species will be near zero at early or late times. Consequently, the fluctuating simulations are stable only at extremely low strength of the fluctuations ($\alpha = 0.002$). There is no significant difference in the evolution of the system at such noise strengths when compared against deterministic simulations. To overcome this, we perform fluctuating simulations with reversibly reacting systems, and where the strength of the fluctuations is initially kept very low at $\alpha = 0.002$, but is

increased by an order of magnitude when the mean concentration of each species is greater than 0.1. The instance where the strength of the fluctuations is increased is shown by the arrow in Fig. 13(a). Thermal fluctuations increase the reaction rate by generating more interfacial area for the reaction to occur. This is reflected in the evolution of $\langle\phi_D\rangle$ in Fig. 13(a). All three fluctuating simulations shown in the figure reach equilibrium faster than the deterministic simulation.

Further, fluctuations are also observed to accelerate the onset of interfacial roughening, as is evidenced by the location of the maxima in the characteristic domain size (Fig. 13(b)). This has been widely hypothesized in experiments, and our simulations confirm this hypothesis. The top inset in Fig. 13(b) depicts the profile of ϕ_{Ad} at the end of one fluctuating simulation, and the bottom inset shows the same profile at equilibrium from the deterministic simulation. The inset suggests that fluctuations are responsible for sustaining the system in an emulsified state. Full strength ($\alpha = 1$) fluctuations are expected to more dramatically accelerate the reaction rate and onset of roughening, and might reveal the existence of a bicontinuous microemulsion near the Lifshitz point [13]. However, we defer such an analysis to a future study. We believe that the study performed here captures the essential physics of thermal fluctuations.

3.6 χN_r parameter

Finally, we quantify the effect of changing the Flory-Huggins interaction parameter, χN_r on the reaction dynamics and intermediate morphology in Fig. 14. The simulations correspond to irreversible reactions with $Da_f = 1$, $(L_x, L_y) = (32, 16)$, and the initial distribution between the homopolymers perturbed by a long wavelength sinusoid. The thickness of the interface decreases with increase in χN_r . Thus, there are fewer contacts between the homopolymers for systems with larger χN_r . Further, the enthalpic penalty for the diffusion of the unlike half of the diblock through an unlike homopolymer domain increases with χN_r . Consequently, the reaction is slower at higher values of χN_r , in agreement with experiments [23]. For $\chi N_r = 4$, the system is in a disordered state upon complete conversion of the homopolymers to diblock, and there are no interfaces left at equilibrium. Systems relaxing to a disordered phase were not observed to spontaneously emulsify, which is consistent with the prediction of an earlier study [7]. It was also reported in that study that when the homopolymers are highly incompatible, with $\chi N_r = 34$, the reactions would be too

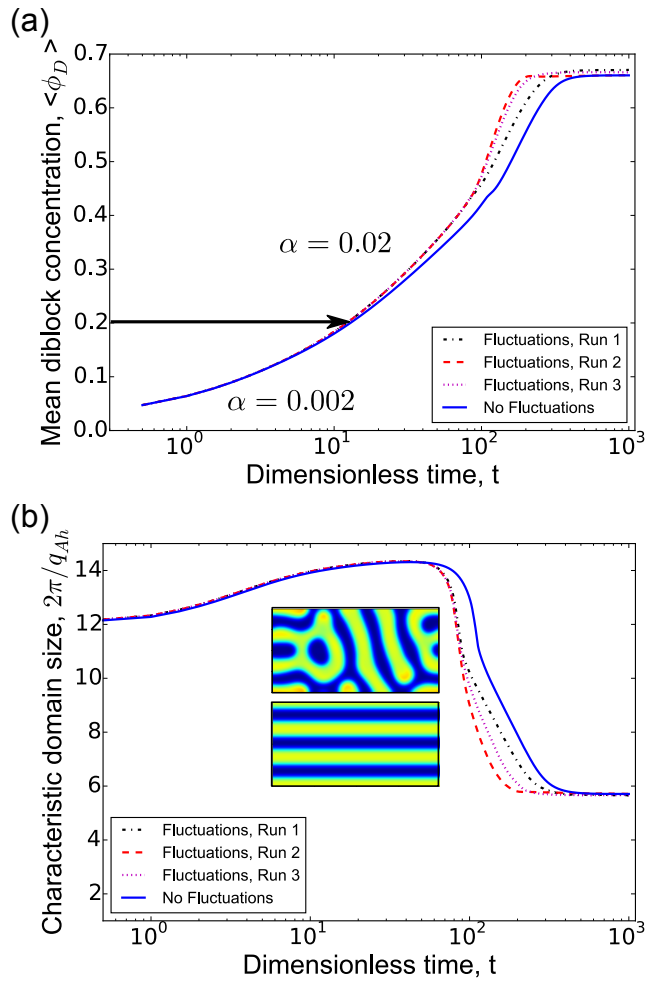


Figure 13: Temporal evolution of (a) mean diblock concentration, and (b) characteristic domain size for simulations with and without fluctuations. The arrow in (a) corresponds to the time where α was increased from 0.002 to 0.02. The top inset in (b) corresponds to the profile of ϕ_{Ad} at the end of a fluctuating simulation, and the bottom inset in (b) shows the profile of ϕ_{Ad} at the end of a simulation with no fluctuations. For all the simulations, $Da_f = 1$, $\chi N_r = 7$, $(L_x, L_y) = (32, 16)$, $K/N_r = 50$, and the initial distribution between the homopolymers is perturbed by a long wavelength sinusoid.

slow to generate enough diblock; consequently, interfacial roughening would not be observed [7]. Unfortunately, we were not able to perform stable simulations at such high χN_r values, but we do observe the time to emulsification to increase with χN_r . Further, the χN_r values where we observe spontaneous emulsification are consistent with the experimental finding.

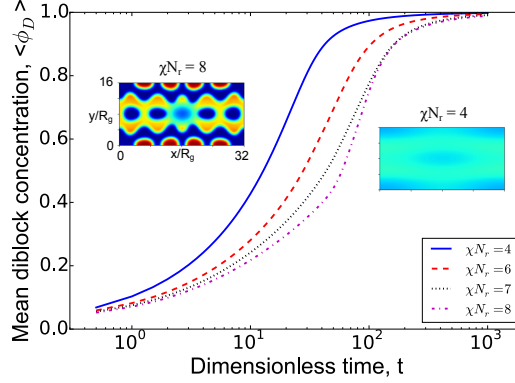


Figure 14: Temporal evolution of the mean diblock concentration as a function of χN_r . The insets show the profile of ϕ_{Ad} at $t = 100$ for $\chi N_r = 8$, and $t = 50$ for $\chi N_r = 4$. For all the simulations, $Da_f = 1$, $(L_x, L_y) = (32, 16)$, the initial distribution between the homopolymers is perturbed by a long wavelength sinusoid, and the reactions are irreversible.

4 Conclusions

We have studied reactive polymer blending by interdiffusion in polymer films, where homopolymers symmetric in chain length and composition undergo an end-coupling reaction to form a symmetric diblock copolymer twice as long as the homopolymers. Using 2-D phase-field simulations, we explored a large parameter space to understand the evolution of reaction dynamics and morphology in such systems, and quantify interfacial roughening and spontaneous emulsification. The reaction dynamics is measured by the reaction rate and mean diblock concentration, and the morphology is quantified by a characteristic domain size obtained from the first moment of the normalized homopolymer structure factor. We find that the dynamics of the system is not significantly influenced by the length of the film or the initial shape of the interface between the polymers, as long as the thickness of the films is constant. The reaction progresses more slowly in thicker films because the reactive homopolymers need to diffuse through a wider domain before reaching the interface where the reaction occurs. Consequently, these films roughen later than thinner films. Systems with inherently faster reaction time scales, quantified by a Damkohler number, Da_f roughen faster, with the roughening time proportional to Da_f^{-1} . The interfacial energy was not observed to drop to negative values at the onset of roughening. Simulations with reversible reactions and systems where a fraction of the homopolymer have reactive end groups show that a critical di-

block concentration exists, below which spontaneous emulsification is not observed. We conclude that roughening is not triggered by the interfacial tension becoming negative, rather it occurs when sufficient copolymer is formed to induce microphase separation to a lamellar microstructure. We also demonstrated that weak thermal fluctuations accelerate the onset of interfacial roughening, and is responsible for maintaining the system in an emulsified state. Finally, we examined the role of the Flory-Huggins interaction parameter, χN_r , and showed that emulsification is only observed in systems which show microphase separation. The reaction is slower at high χN_r , consequently, the time to observe emulsification increases with χN_r .

Conflicts of Interest

There are no conflicts to declare.

R.S. acknowledges financial support from Koninklijke DSM N.V. This work was partially supported by the MRSEC Program of the National Science Foundation under Award No. DMR 1720256 (IRG-3). We also acknowledge the use of the Center for Scientific Computing, supported by the California NanoSystems Institute, the NSF MRSEC (DMR 1720256) and NSF CNS 1725797.

References

- [1] Macosko CW, Jeon HK, Hoyer TR. Reactions at polymer–polymer interfaces for blend compatibilization. *Prog Polym Sci.* 2005;30(8-9):939–947.
- [2] Jeon HK, Zhang J, Macosko CW. Premade vs. reactively formed compatibilizers for PMMA/PS melt blends. *Polymer.* 2005;46(26):12422–12429.
- [3] Koning C, Van Duin M, Pagnoulle C, Jerome R. Strategies for compatibilization of polymer blends. *Prog Polym Sci.* 1998;23(4):707–757.
- [4] Shull KR, Kellock AJ, Deline VR, MacDonald SA. Vanishing interfacial tension in an immiscible polymer blend. *J Chem Phys.* 1992;97(3):2095–2104.
- [5] Jiao J, Kramer EJ, de Vos S, Möller M, Koning C. Polymer interface instability caused by a grafting reaction. *Polymer.* 1999;40(12):3585–3588.
- [6] Jiao J, Kramer EJ, de Vos S, Möller M, Koning C. Morphological changes of a molten polymer/polymer interface driven by grafting. *Macromolecules.* 1999;32(19):6261–6269.
- [7] Lyu SP, Cernohous JJ, Bates FS, Macosko CW. Interfacial reaction induced roughening in polymer blends. *Macromolecules.* 1999;32(1):106–110.
- [8] Kim BJ, Kang H, Char K, Katsov K, Fredrickson GH, Kramer EJ. Interfacial roughening induced by the reaction of end-functionalized polymers at a PS/P2VP interface: Quantitative analysis by DSIMS. *Macromolecules.* 2005;38(14):6106–6114.
- [9] Zhang J, Lodge TP, Macosko CW. Interfacial morphology development during PS/PMMA reactive coupling. *Macromolecules.* 2005;38(15):6586–6591.
- [10] Épinat C, Trouillet-Fonti L, Jéol S, Long DR, Sotta P. Nucleation and Growth of Ordered Copolymer Structures at Reactive Interfaces between PA6 and MA-g-HDPE. *ACS Macro Lett.* 2015;4(5):488–491.
- [11] Broseta D, Fredrickson GH. Phase equilibria in copolymer/homopolymer ternary blends: Molecular weight effects. *J Chem Phys.* 1990;93(4):2927–2938.

- [12] Janert PK, Schick M. Phase behavior of ternary homopolymer/diblock blends: Influence of relative chain lengths. *Macromolecules*. 1997;30(1):137–144.
- [13] Bates FS, Maurer WW, Lipic PM, Hillmyer MA, Almdal K, Mortensen K, et al. Polymeric bicontinuous microemulsions. *Phys Rev Lett*. 1997;79(5):849.
- [14] Janert PK, Schick M. Phase behavior of binary homopolymer/diblock blends: Temperature and chain length dependence. *Macromolecules*. 1998;31(4):1109–1113.
- [15] Pernot H, Baumert M, Court F, Leibler L. Design and properties of co-continuous nanostructured polymers by reactive blending. *Nat Mater*. 2002;1(1):54–58.
- [16] Fredrickson GH. Diffusion-controlled reactions at polymer-polymer interfaces. *Phys Rev Lett*. 1996;76(18):3440.
- [17] O'shaughnessy B, Sawhney U. Polymer reaction kinetics at interfaces. *Phys Rev Lett*. 1996;76(18):3444.
- [18] Fredrickson GH, Milner ST. Time-dependent reactive coupling at polymer- polymer interfaces. *Macromolecules*. 1996;29(23):7386–7390.
- [19] Fredrickson GH, Leibler L. Theory of diffusion-controlled reactions in polymers under flow. *Macromolecules*. 1996;29(7):2674–2685.
- [20] Guégan P, Macosko C, Ishizone T, Hirao A, Nakahama S. Kinetics of chain coupling at melt interfaces. *Macromolecules*. 1994;27(18):4993–4997.
- [21] Orr C, Cernohous J, Guegan P, Hirao A, Jeon H, Macosko C. Homogeneous reactive coupling of terminally functional polymers. *Polymer*. 2001;42(19):8171–8178.
- [22] Yin Z, Koulic C, Pagnouille C, Jérôme R. Probing of the reaction progress at a PMMA/PS interface by using anthracene-labeled reactive PS chains. *Langmuir*. 2003;19(2):453–457.
- [23] Jones TD, Schulze JS, Macosko CW, Lodge TP. Effect of thermodynamic interactions on reactions at polymer/polymer interfaces. *Macromolecules*. 2003;36(19):7212–7219.

- [24] Orr CA, Adedeji A, Hirao A, Bates FS, Macosko CW. Flow-induced reactive self-assembly. *Macromolecules*. 1997;30(4):1243–1246.
- [25] Milner ST, Xi H. How copolymers promote mixing of immiscible homopolymers. *Journal of rheology*. 1996;40(4):663–687.
- [26] Bironeau A, Salez T, Miquelard-Garnier G, Sollogoub C. Existence of a critical layer thickness in PS/PMMA nanolayered films. *Macromolecules*. 2017;50(10):4064–4073.
- [27] Feng J, Zhang Z, Bironeau A, Guinault A, Miquelard-Garnier G, Sollogoub C, et al. Breakup behavior of nanolayers in polymeric multilayer systems—Creation of nanosheets and nanodroplets. *Polymer*. 2018;143:19–27.
- [28] Lu B, Alcouffe P, Sudre G, Pruvost S, Serghei A, Liu C, et al. Unveiling the Effects of In Situ Layer–Layer Interfacial Reaction in Multilayer Polymer Films via Multilayered Assembly: From Microlayers to Nanolayers. *Macromol Mater Eng*. 2020;305(5):2000076.
- [29] Yeung C, Herrmann KA. Molecular dynamics simulation of reactive compatibilization of polymer blends. *Macromolecules*. 2003;36(1):229–237.
- [30] Berezkin AV, Kudryavtsev YV. Simulation of end-coupling reactions at a polymer–polymer interface: The mechanism of interfacial roughness development. *Macromolecules*. 2011;44(1):112–121.
- [31] Berezkin AV, Guseva DV, Kudryavtsev YV. Formation of Linear and Graft Block Copolymers at a Polymer/Polymer Interface: How Copolymer Brush and Microdomain Morphology Control Heterogeneous Reactions. *Macromolecules*. 2012;45(21):8910–8920.
- [32] Berezkin AV, Kudryavtsev YV. End-coupling reactions in incompatible polymer blends: from droplets to complex micelles through interfacial instability. *Macromolecules*. 2013;46(12):5080–5089.
- [33] Cheng MH, Balazs AC, Yeung C, Ginzburg VV. Modeling reactive compatibilization of a binary blend with interacting particles. *J Chem Phys*. 2003;118(19):9044–9052.

- [34] Tikekar M, Delaney KT, Villet M, Tree DR, Fredrickson GH. A phase field model for dynamic simulations of reactive blending of polymers. *Soft Matter*. 2022;.
- [35] Tree DR, Delaney KT, Cenicerros HD, Iwama T, Fredrickson GH. A multi-fluid model for microstructure formation in polymer membranes. *Soft Matter*. 2017;13(16):3013–3030.
- [36] Uneyama T, Doi M. Density functional theory for block copolymer melts and blends. *Macromolecules*. 2005;38(1):196–205.
- [37] Liu JV, García-Cervera CJ, Delaney KT, Fredrickson GH. Optimized phase field model for diblock copolymer melts. *Macromolecules*. 2019;52(7):2878–2888.
- [38] Khatavkar VV, Anderson PD, Duineveld PC, Meijer HH. Diffuse interface modeling of droplet impact on a pre-patterned solid surface. *Macromol Rapid Commun*. 2005;26(4):298–303.
- [39] Khatavkar V, Anderson P, Duineveld P, Meijer H. Diffuse-interface modelling of droplet impact. *J Fluid Mech*. 2007;581(97):29.
- [40] Cromer M, Villet MC, Fredrickson GH, Leal LG. Shear banding in polymer solutions. *Phys Fluids*. 2013;25(5):051703.
- [41] Peterson JD, Cromer M, Fredrickson GH, Gary Leal L. Shear banding predictions for the two-fluid Rolie-Poly model. *J Rheol*. 2016;60(5):927–951.
- [42] Peterson JD, Fredrickson GH, Leal LG. Does shear induced demixing resemble a thermodynamically driven instability? *J Rheol*. 2019;63(2):335–359.
- [43] Tree DR, Iwama T, Delaney KT, Lee J, Fredrickson GH. Marangoni flows during nonsolvent induced phase separation. *ACS Macro Lett*. 2018;7(5):582–586.
- [44] Tree DR, Dos Santos LF, Wilson CB, Scott TR, Garcia JU, Fredrickson GH. Mass-transfer driven spinodal decomposition in a ternary polymer solution. *Soft matter*. 2019;15(23):4614–4628.

- [45] Garcia JU, Iwama EYC, Tree DR, Delaney KT, Fredrickson GH. Mechanisms of asymmetric membrane formation in nonsolvent-induced phase separation. *ACS Macro Lett.* 2020;9:1617–1624.
- [46] Doi M, Onuki A. Dynamic coupling between stress and composition in polymer solutions and blends. *J Phys II.* 1992;2(8):1631–1656.
- [47] Fogler HS. *Elements of chemical reaction engineering.* Pearson Educación. 1999;.
- [48] Hohenberg PC, Halperin BI. Theory of dynamic critical phenomena. *Rev Mod Phys.* 1977;49(3):435.
- [49] Jones RAL. *Soft condensed matter.* Oxford University Press. 2002;.
- [50] Leibler L. Theory of microphase separation in block copolymers. *Macromolecules.* 1980;13(6):1602–1617.
- [51] Ohta T, Kawasaki K. Equilibrium morphology of block copolymer melts. *Macromolecules.* 1986;19(10):2621–2632.
- [52] Lacasta A, Hernández-Machado A, Sancho JM, Toral R. Domain growth in binary mixtures at low temperatures. *Phys Rev B: Condens Matter.* 1992;45(10):5276.
- [53] Badalassi VE, Cenicerros HD, Banerjee S. Computation of multiphase systems with phase field models. *J Comput Phys.* 2003;190(2):371–397.
- [54] Chandler D. *Introduction to modern statistical mechanics.* Oxford University Press, Oxford, UK. 1987;40.
- [55] Butt HJ, Graf K, Kappl M. *Physics and chemistry of interfaces.* John Wiley & Sons; 2013.